Membrane-free Electrocatalysis of CO_2 to C_2 on CuO/CeO_2 Nanocomposites

Yangming Tian, Xiang Fei, Hui Ning*, Wenhang Wang, Xiaojie Tan, Xiaoshan Wang, Zhengguang Ma, Zhihao Guo and Mingbo Wu*

College of Chemical Engineering, College of New Energy, Institute of New Energy, State Key Laboratory of Heavy Oil Processing, China University of Petroleum (East China), Qingdao, china

Carbon dioxide electroreduction (CO_2RR) with renewable energy is of great significance to realize carbon neutralization. Traditional electrolysis devices usually need an ion exchange membrane to eliminate the interference of oxygen generated on the anode. Herein, the novel CuO/CeO_2 composite was facilely prepared by anchoring small CuO nanoparticles on the surface of CeO_2 nanocubes. In addition, CuO(002) crystal planes were induced to grow on CeO_2(200), which was preferable for CO_2 adsorption and C-C bond formation. As the catalyst in a membrane-free cell for CO_2RR, the Cu^+ was stabilized due to strong interactions between copper and ceria to resist the reduction of negative potentials and the oxidation of oxygen from the counter electrode. As a result, a high Faradaic efficiency of 62.2% toward C_2 products (ethylene and ethanol) was achieved for the first time in the membrane-free conditions. This work may set off a new upsurge to drive the industrial application of CO_2RR through membrane-free electrocatalysis.

Keywords: carbon dioxide, membrane free, electrocatalysis, copper, ceria

HIGHLIGHT

- Nano CeO2 cube was applied as supports for highly dispersed CuO nanoparticles.
- The CuO(002) crystal faces were preferentially grown on CeO2(200).
- The Faradaic efficiency of CO_2 to C_2 exceeds 62% in a membrane-free cell.

INTRODUCTION

Carbon dioxide electroreduction reaction (CO_2RR) has attracted worldwide attention because of its promising application in suppressing carbon dioxide emission (Gong et al., 2019; Fan et al., 2020; Li H et al., 2021; Sun et al., 2021; Zhao et al., 2021; Li et al., 2022). However, it still needs high performance catalysts to accelerate the conversion of carbon dioxide and control the selectivity of products for the industrial application.

On different catalysts, various products may be obtained, such as carbon monoxide, formic acid, methanol, methane, ethylene, ethanol, oxalic acid, and acetic acid. Among them, the C_2+ products were desired because of their much higher added value and more important theoretical significance of understanding C-C bond formation (Ma et al., 2020; Li Z et al., 2021; Zhang et al., 2021). Among all the elements, copper is considered as the only candidate as a high selective catalyst for C_2+ products. In order to achieve better catalytic performance of copper-based catalysts, tremendous

works have been carried out from the aspect of crystal faces (Suen et al., 2019), size (Wang et al., 2019), morphology (De Luna et al., 2018), defects (Gu et al., 2021), valence state (Mistry et al., 2016), and surface modification (Li F et al., 2020). Unfortunately, nearly all the pioneer works are executed in a two-chamber cell system, which need a cation or anion exchange membrane to separate the anode and cathode chambers. From a practical and industrial point of view, membranes make the CO_2RR reactor more complex, increase cost, and limits large-scale application. Therefore, the design of a membrane-free electroreduction process is of great significance. Though with more concise and compact structure, the membrane-free cell still faces several critical challenges, such as the separation of products and the coupling with anodic reaction. For instance, the water oxidation reaction is inevitably on the anode when using aqueous electrolyte. In this condition, the oxygen produced and dissolved in the electrolyte may oxidize the active sites and lead to the decomposition of products in the liquid phase. In order to improve the oxygen tolerance of catalysts for CO_2RR, several interesting works have been reported (Lu et al., 2019; He et al., 2020). For example, Sun et al. (Li P et al., 2020) developed a CO_2-selective layer by introducing aniline into the pores of a microporosity polymer to permeate CO_2 from O_2 mixture. It was found that the acid–base interaction between CO_2 and aniline enhances CO_2 separation from O_2. Even if the polymer coating is a feasible strategy to protect the active sites from interacting with oxygen, it is not conducive to the effective exposure of active sites. Therefore, new strategies need to be developed to achieve oxygen tolerance and full exposure of active sites simultaneously.

In addition to oxidation, the reduction of active sites in the CO_2RR process also needs to be considered, whether there is a membrane or not. Especially for the oxide-derived copper (OD-Cu) catalysts, the Cu^+ has been proposed as the most important active site in the formation of C-C bond, while its stability has always been a great challenge due to its easy reduction under negative applied potentials in the CO_2RR procedure (Yuan et al., 2018). The strong metal–support interactions have been proved a promising way to improve catalytic activity of metal active sites, which is also applied to upgrade the catalytic performance of copper-based catalysts for the CO_2RR (Geioushy et al., 2017). For example, Lee et al. (2019) sintered the CuO nanocrystals onto CeO_2 and found that the ceria is proposed to weaken the hydrogen binding energy of adjacent Cu sites to stabilize the *OCCO intermediate *via* an additional chemical interaction with an oxygen atom in the *OCCO. Zheng et al. (Wang et al., 2018) designed single-atomic Cu–substituted mesoporous CeO_2 nanorods with multiple oxygen vacancy bond. They found each Cu atom substituted in the CeO_2(110) surface can be stabilized by coordinating with three oxygen vacancies, yielding a highly effective catalytic center for CO_2 adsorption and activation to methane. On the contrary, Qiao et al. (Wu et al., 2018) proved the isolated cuprous ions doped in ceria nanorods exhibit strong capability to capture CO_2 and CO molecules and decrease the energy barrier for producing C_2 products, leading to a high Faradaic efficiency (FE) of 47.6% toward ethylene. On the other hand, the stabilization effects of ceria substrate toward cuprous ions are responsible for the long-term durability. Sun

et al. (Chu et al., 2020a) found that the selectivity and activity of the CO_2RR on Cu/CeO_2 composites are depended strongly on the exposed crystal facets of CeO_2. By tuning the CuO/CeO_2 interfacial interaction, they further improved the selectivity of ethylene by stabilizing Cu^+ at the $CuO–CeO_2$ interface (Chu et al., 2020b). Han et al. (Yan et al., 2021) modified copper oxide with cerium oxide to enhanced water activation and accelerate the formation rate of *CHO, thus enhance the selectivity and activity of C_{2+} products by promoting the hydrogenation of *CHO. Though the existing works have proved that CeO_2 is a promising candidate as the supports of copper in the traditional H-cell (with a membrane to separate two champers) for the CO_2RR process, few works have been reported achieving a high selectivity toward C_2 products in a membrane-free cell.

Herein, we synthesized a series of novel CuO/CeO_2 composites by dispersing CuO nanoparticles (NPs) on CeO_2 nonocubes (NCs), which is then used as catalysts for the CO_2RR in a single chamber cell without membrane. Surprisingly, the Faradaic efficiency of C_2 was found exceeding 62% for the first time. This new finding may set off a new research climax in a simple membrane-free cell for industrial perspective of CO_2 electrocatalysis.

RESULTS AND DISCUSSION

The fabrication of CuO/CeO_2 is illustrated in **Figure 1**. The CeO_2 NCs were synthesis by a modified hydrothermal method (Zhu et al., 2020). Through an impregnation–precipitation process, copper (II) ions were introduced into ceria lattice. After annealing at 773 K for 3 h, the CuO/CeO_2 samples were obtained. The detailed composition of CuO/CeO_2 composites is listed in **Supplementary Table S1**.

The crystal structure of samples as made was firstly investigated by XRD. As depicted in **Figure 2A**, the characteristic peaks of 28.6°, 33.1°, 47.5°, and 56.4° were ascribed to the (111), (200), (220) and (311) planes of CeO_2, which is accurately corresponds to the standard spectrum of CeO_2 (JCPDS No.03-065-0459, space group: Fd-3m Ia$\bar{3}$, a = 10.774 Å). As a control experiment, we also synthesized CuO following the same procedure but in the absence of CeO_2. The peaks at 38.8° was corresponded to the (111) planes of CuO (JCPDS No.80-1916). Interestingly, no characteristic peaks of CuO or Cu_2O were found in the CuO/CeO_2 composites, which need further characterization.

The detailed element composition of CuO/CeO_2 was analyzed by XPS spectrum. In **Figure 2B**, the characteristic peaks of Cu, Ce, and O elements were observed clearly, indicating that the CuO/CeO_2 composites were successful prepared. The high-resolution XPS spectrum of Ce elopement is shown in **Figure 2C**. The Ce 3d curve was fitted to 10 peaks corresponding to Ce $3d_{5/2}$ (μ_1, 880.5 eV; ν_o, 882.2 eV; μ_0, 884.1 eV; ν_1,888.7 eV; and ν_2, 897.8 eV) and Ce $3d_{3/2}$ state (μ_1', 898.4 eV; ν_0', 900.7 eV; μ_0', 902.5 eV; ν_1', 907.5 eV; and ν_2', 916.6 eV). The peaks of μ_0, μ_1, μ_0', and μ_1' are attributed to Ce^{3+} species, and the remaining peaks are attributed to the Ce^{4+}
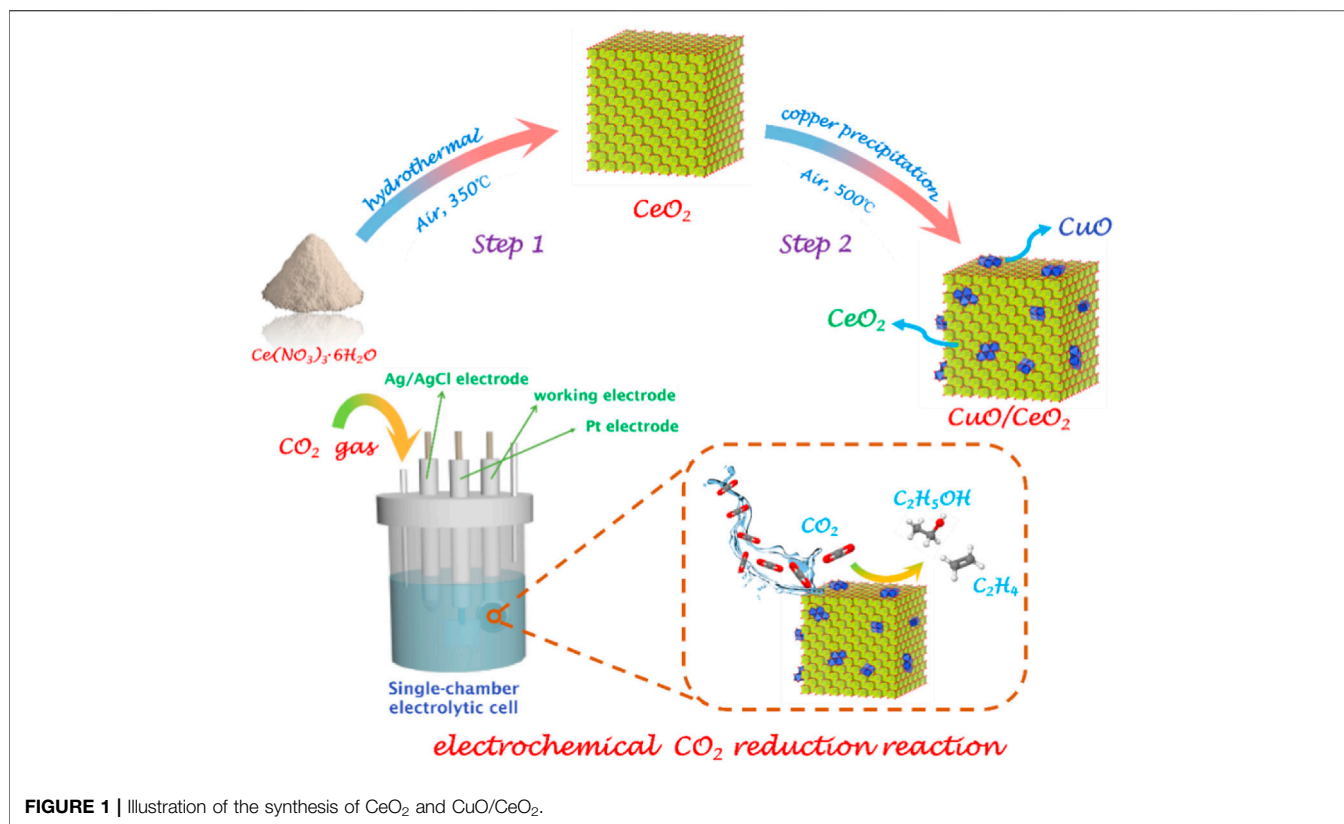
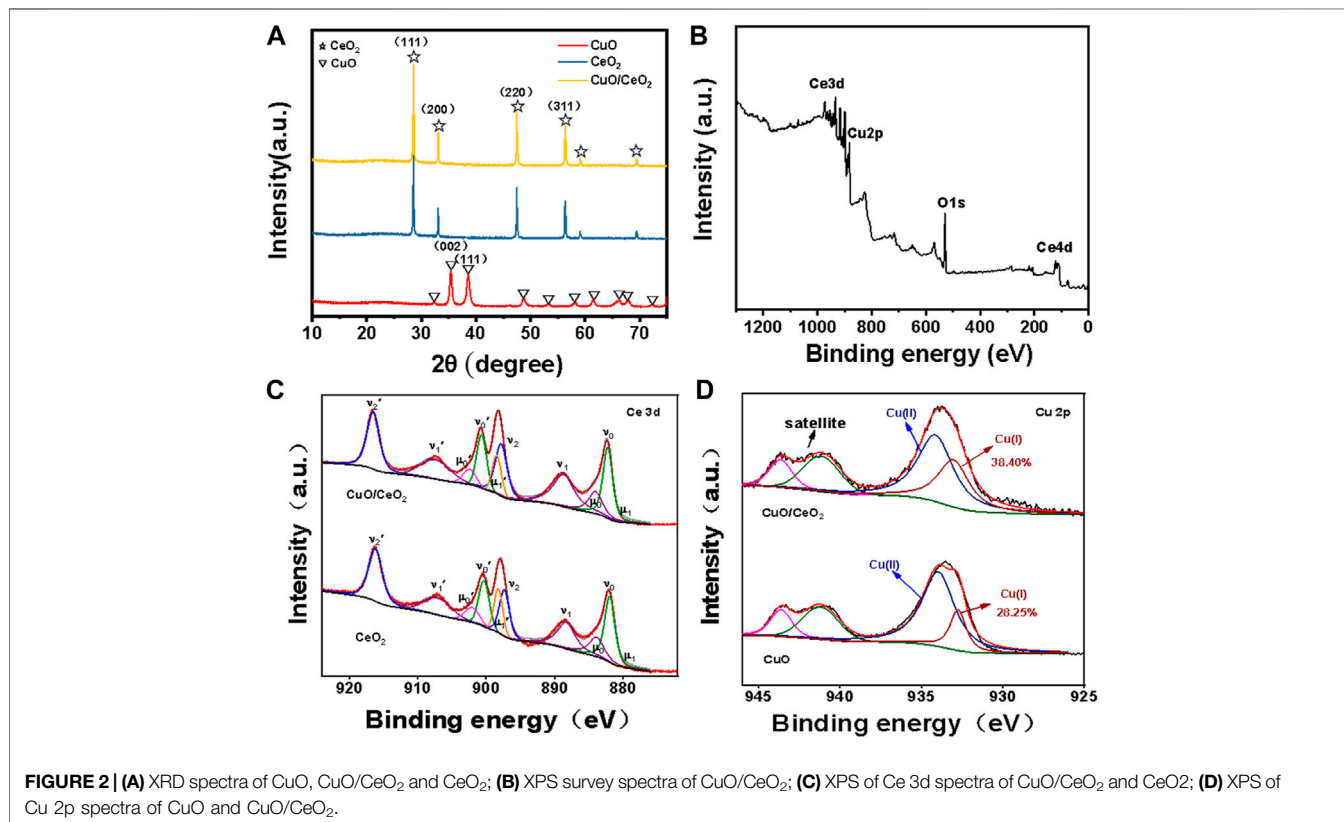FIGURE 1 | Illustration of the synthesis of CeO$_2$ and CuO/CeO$_2$.

FIGURE 2 | (A) XRD spectra of CuO, CuO/CeO$_2$ and CeO$_2$; (B) XPS survey spectra of CuO/CeO$_2$; (C) XPS of Ce 3d spectra of CuO/CeO$_2$ and CeO2; (D) XPS of Cu 2p spectra of CuO and CuO/CeO$_2$.
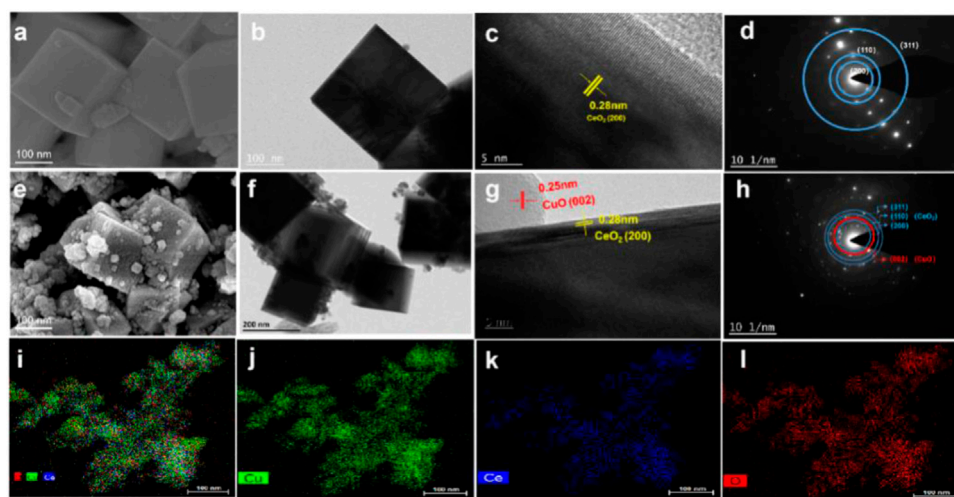
FIGURE 3 | (A) SEM images of CeO_2; **(B)** TEM images of CeO_2; **(C)** HRTEM images of CeO_2; **(D)** SAED pattern of CeO_2; **(E)** SEM images of CuO/CeO_2; **(F)** TEM images of CuO/CeO_2; **(G)** HRTEM images of CuO/CeO_2; **(H)** SAED pattern of CuO/CeO_2; **(I–L)** EDS mapping of CuO/CeO_2.
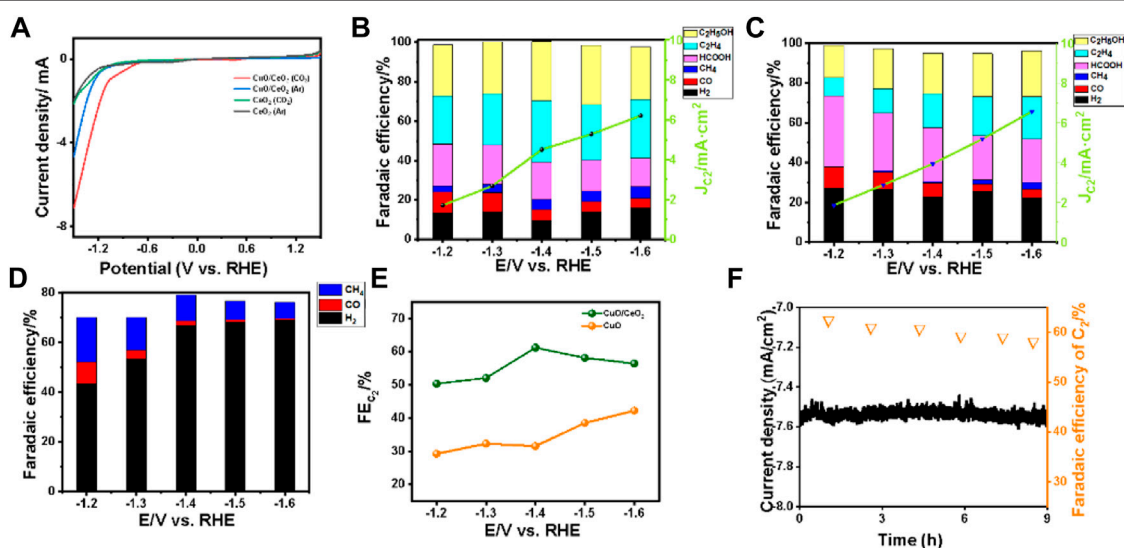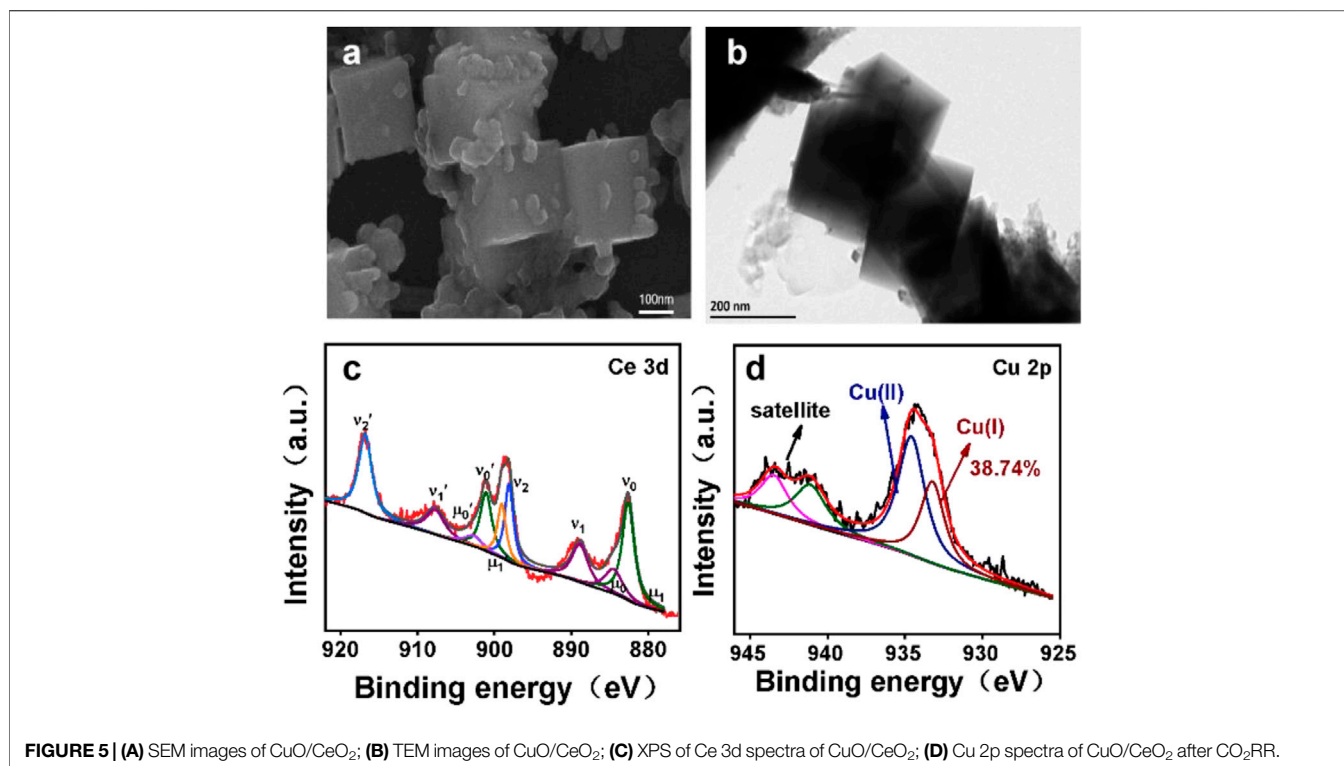

FIGURE 4 | (A) LSV curves of CeO_2 and CuO/CeO_2 under Ar- and CO_2-saturated 0.1 M $KHCO_3$ in a single cell; **(B)** Faradaic efficiency and C_2 products current density of CuO/CeO_2; **(C)** Faradaic efficiency and C_2 products current density of CuO; **(D)** Faradaic efficiency of CeO_2; **(E)** Comparison of Faraday efficiency of CuO/CeO_2 and CuO at different voltages; **(F)** stability curve and Faradaic efficiency of C_2 during 9 h.

species (Wang et al., 2018). According to the peak area ratio of the Ce 3d region of CuO/CeO_2, the relative Ce^{3+} percentage in CeO_2 is 17.6%, which is much less than that in the pure CeO_2 (20.8% of Ce^{3+}). This phenomenon is derived from the substitution of Ce ions by Cu ions during the synthesis procedure (Wu et al., 2018). The Cu 2p spectra of CuO/CeO_2 and CuO show distinct copper oxide features in **Figure 2D**. In addition to the satellite peaks of Cu^{2+}, the binding energies (BEs) of 934.2 eV in the Cu $2p_{3/2}$ region can be attributed to the Cu^{2+} and the peak at 932.7 eV is attributed to the Cu^+ (Lei et al., 2020) According to the peak area ratio of copper oxidation states in the Cu $2p_{3/2}$ region, the relative

Cu^+ percentage of CuO dispersed on CeO_2 is determined to be 38.4%, while the relative Cu^+ percentage of pure copper oxide is 28.3%. The increased content of Cu^+ was derived from the transfer of electrons from Ce^{3+} to Cu^{2+} (Chu et al., 2020b).

The morphology of CuO/CeO_2 was verified by the SEM and TEM images. As shown in **Figure 3A**, the CeO_2 NPs obtained in this work have an obviously cubic morphology with smooth surface, which size is ca. 23 nm. The morphology of CeO_2 was confirmed by TEM (**Figure 3B**) to be classical cubes with clear boundaries. In the HRTEM image, the $CeO_2(200)$ crystal planes were mainly exposed (**Figure 3C**), which is confirmed by the

FIGURE 5 | (A) SEM images of CuO/CeO$_2$; **(B)** TEM images of CuO/CeO$_2$; **(C)** XPS of Ce 3d spectra of CuO/CeO$_2$; **(D)** Cu 2p spectra of CuO/CeO$_2$ after CO$_2$RR.

SAED pattern (**Figure 3D**). After compositing with CuO, the cubic morphology and size of CeO$_2$ was maintained but the smooth surface was mostly covered by the irregular CuO NPs with the diameter from 20 to 30 nm (**Figures 3E,F**).

It is worth noting that there is a clear boundary between CuO(002) and CeO$_2$(200), as shown in **Figure 3G**. Furthermore, the SAED pattern of CuO/CeO$_2$ (**Figure 3H**) confirmed that the CeO$_2$(200) and CuO(002) planes exist simultaneously and the EDS mapping (**Figures 3I–L**) indicates the CuO NPs were uniformly dispersed on CeO$_2$.

To verify the catalytic performance of the catalysts as made, the LSV curves of all the samples in 0.1 M KHCO$_3$ with Ar- and CO$_2$-saturated were recorded, as shown in **Figure 4A**. For the CuO/CeO$_2$, larger current density was obtained in CO$_2$-saturated 0.1 M KHCO$_3$ than in the Ar-saturated conditions, indicating the CuO/CeO$_2$ composites have obviously catalytic activity toward CO$_2$RR (Chu et al., 2020b). As a control example, the LSV curves of CeO$_2$ almost coincide in the Ar- and CO$_2$-saturated conditions, indicating the ceria has no activity toward CO$_2$RR.

Furthermore, the comprehensive catalytic performance of CO$_2$RR on CuO/CeO$_2$ under different applied potentials was investigated in a home-made single chamber electrolytic cell without membrane (**Supplementary Figure S1**). The Faradaic efficiencies of all the products were recorded in **Figures 4B–D**. Only a small amount of CO and methane were detected in the gas products, which means the CeO$_2$ as catalyst has low activity toward CO$_2$ electroreduction. While for the CuO/CeO$_2$ samples, various products were detected by chromatography, including CO, CH$_4$, C$_2$H$_4$, C$_2$H$_5$OH, and HCOOH. Take C$_2$ (C$_2$H$_4$ + C$_2$H$_5$OH) as the target product, as shown in **Figures 4C,F**, the maximum Faraday efficiency of C$_2$ always appears at −1.4 V vs. the reversible hydrogen electrode (RHE) and the FE of C$_2$ arrived at the highest value of 62.2%. As control experiments, the maximum FE of C$_2$ on pristine CuO under −1.4 V vs. RHE is only 40%, indicating the CeO$_2$ as supports can increase the selectivity of CuO toward CO$_2$ electroreduction to C$_2$. For comparison, the FEs of products on the mixture of CuO and CeO$_2$ (with the same ratio of Cu/Ce as CuO/CeO$_2$) were also recorded and depicted in **Supplementary Figure S3**. The FE of C$_2$ is 51.1% at −1.4 V vs. RHE, which is lower than that of CuO/CeO$_2$ but higher than that of CuO, proving that the presence of CeO$_2$ is conducive to the selectivity of C$_2$ while the composited state of CuO and CeO$_2$ has better performance in producing C$_2$ products than the mixed state. Next, the partial current density was applied to evaluate the formation rate of target products. Specially at −1.4 V vs. RHE, the partial current density of C$_2$ is 4.5 mA cm$^{−2}$ on CuO/CeO$_2$, which is higher than that on CuO (3.9 mA cm$^{−2}$). While in the H-type cell, with the optimum CuO/CeO$_2$ catalyst, the FE of C$_2$ is 58.4% with a partial current density of 4.3 mA cm$^{−2}$, as shown in **Supplementary Figure S4**. The higher selectivity and activity further prove the superiority of our catalyst in a single cell than the H-type cell.

We also tested the long-time durability of different catalysts in the membrane-free condition (**Figure 4F** and **Supplementary Figure S5**). After 9 h' electrocatalysis at −1.4 V vs. RHE, the catalytic performance of CuO/CeO$_2$ is stable with no significant change and the Faradaic efficiency for C$_2$ remains around 60%. On the contrary, when the pristine CuO was used as catalyst, the current density had a noticeable increasing over time and the FE of C$_2$ decreased from 40 to 21%, which mean the Cu$^+$ in CuO cannot be stabilized and the selectivity of C$_2$ was synchronously reduced.

In order to unveil the reason of different performance between CuO/CeO_2 and pristine CuO, the composition and morphology of catalyst after electrocatalysis were characterized. As proved by SEM and TEM image in **Figures 5A,B**, the morphology of CuO/CeO_2 was well maintained after reaction. In addition, the XPS results further revealed that the ratio of $Cu^+/(Cu^+ + Cu^{2+})$ has no significant change compared to the fresh catalyst, indicates Cu^+ can be well stabilized by CeO_2 during the CO_2RR process. The stability of the morphology and valence state of the CuO/CeO_2 composite further proves that the stabilization effects of ceria toward Cu^+, which provides favorable catalysts for the high-efficiency electroreduction of carbon dioxide in a membrane-free electrolyzer.

CONCLUSION

In this work, the CeO_2 NCs with average size of 230 nm were facilely synthesized by a hydrothermal method. Further through an impregnation–calcination process, the CuO NPs with diameters from 20 to 30 nm was highly dispersed on the surface of CeO_2 to fabricate novel composites of CuO/CeO_2, in which the mainly exposed crystal faces was $CuO(002)$ and $CeO_2(200)$. Due to the strong metal–metal oxide interaction between copper and ceria, the content of Cu^+ was increased in the CuO/CeO_2 composite and stabilized in the CO_2RR process, which makes the CuO/CeO_2 an excellent catalyst for CO_2RR toward C_2 products with high selectivity and stability in a single cell without membrane. This study opens up a new way to realize the high-efficiency electroreduction of CO_2 by using a simple membrane-free system.

REFERENCES

Chu, S., Li, X., W. Robertson, A., and Sun, Z. (2020a). Electrocatalytic CO_2 Reduction to Ethylene over CeO_2-Supported Cu Nanoparticles: Effect of Exposed Facets of CeO_2. *Acta Phys. Chim. Sin.* 37, 2009023–2009020. doi:10.3866/pku.whxb202009023

Chu, S., Yan, X., Choi, C., Hong, S., Robertson, A. W., Masa, J., et al. (2020b). Stabilization of Cu^+ by Tuning a CuO-CeO_2 Interface for Selective Electrochemical CO_2 Reduction to Ethylene. *Green Chem.* 22, 6540–6546. doi:10.1039/d0gc02279a

De Luna, P., Quintero-Bermudez, R., Dinh, C.-T., Ross, M. B., Bushuyev, O. S., Todorović, P., et al. (2018). Catalyst Electro-Redeposition Controls Morphology and Oxidation State for Selective Carbon Dioxide Reduction. *Nat. Catal.* 1, 103–110. doi:10.1038/s41929-017-0018-9

Fan, Q., Hou, P., Choi, C., Wu, T. S., Hong, S., Li, F., et al. (2020). Activation of Ni Particles into Single Ni-N Atoms for Efficient Electrochemical Reduction of CO_2. *Adv. Energy Mat.* 10, 1903068. doi:10.1002/aenm.201903068

Geioushy, R. A., Khaled, M. M., Alhooshani, K., Hakeem, A. S., and Rinaldi, A. (2017). Graphene/ZnO/Cu_2O Electrocatalyst for Selective Conversion of CO_2 into N-Propanol. *Electrochimica Acta* 245, 456–462. doi:10.1016/j.electacta.2017.05.185

Gong, Q., Ding, P., Xu, M., Zhu, X., Wang, M., Deng, J., et al. (2019). Structural Defects on Converted Bismuth Oxide Nanotubes Enable Highly Active Electrocatalysis of Carbon Dioxide Reduction. *Nat. Commun.* 10, 2807. doi:10.1038/s41467-019-10819-4

Gu, Z., Shen, H., Chen, Z., Yang, Y., Yang, C., Ji, Y., et al. (2021). Efficient Electrocatalytic CO_2 Reduction to C_{2+} Alcohols at Defect-Site-Rich Cu Surface. *Joule* 5, 429–440. doi:10.1016/j.joule.2020.12.011

DATA AVAILABILITY STATEMENT

The original contributions presented in the study are included in the article/**Supplementary Material**; further inquiries can be directed to the corresponding authors.

AUTHOR CONTRIBUTIONS

YT: experiments and writing. XF and DFT: calculation. HN: experimental guidance. WW: experimental assistant. XT: experimental assistant. XW: experimental assistant. ZM: experimental assistant. ZG: experimental assistant. MW: article review.

FUNDING

SUPPLEMENTARY MATERIAL

The Supplementary Material for this article can be found online at: https://www.frontiersin.org/articles/10.3389/fchem.2022.915759/full#supplementary-material

He, M., Li, C., Zhang, H., Chang, X., Chen, J. G., Goddard, W. A., 3rd, et al. (2020). Oxygen Induced Promotion of Electrochemical Reduction of CO_2 via Co-electrolysis. *Nat. Commun.* 11, 3844. doi:10.1038/s41467-020-17690-8

Lee, C. W., Shin, S.-J., Jung, H., Nguyen, D. L. T., Lee, S. Y., Lee, W. H., et al. (2019). Metal-Oxide Interfaces for Selective Electrochemical C-C Coupling Reactions. *ACS Energy Lett.* 4, 2241–2248. doi:10.1021/acsenergylett.9b01721

Lei, Q., Zhu, H., Song, K., Wei, N., Liu, L., Zhang, D., et al. (2020). Investigating the Origin of Enhanced C_{2+} Selectivity in Oxide-/Hydroxide-Derived Copper Electrodes during CO_2 Electroreduction. *J. Am. Chem. Soc.* 142, 4213–4222. doi:10.1021/jacs.9b11790

Li, F., Thevenon, A., Rosas-Hernández, A., Wang, Z., Li, Y., Gabardo, C. M., Ozden, A., Dinh, C. T., Li, J., Wang, Y., Edwards, J. P., Xu, Y., McCallum, C., Tao, L., Liang, Z.-Q., Luo, M., Wang, X., Li, H., O'Brien, C. P., Tan, C.-S., Nam, D.-H., Quintero-Bermudez, R., Zhuang, T.-T., Li, Y. C., Han, Z., Britt, R. D., Sinton, D., Agapie, T., Peters, J. C., and Sargent, E. H. (2020). Molecular Tuning of CO_2-to-ethylene Conversion. *Nature* 577, 509–513. doi:10.1038/s41586-019-1782-2

Li, H., Liu, T., Wei, P., Lin, L., Gao, D., Wang, G., et al. (2021). High-Rate CO_2 Electroreduction to C_{2+} Products over a Copper-Copper Iodide Catalyst. *Angew. Chem. Int. Ed.* 60, 14329–14333. doi:10.1002/anie.202102657

Li, P., Lu, X., Wu, Z., Wu, Y., Malpass-Evans, R., McKeown, N. B., et al. (2020). Acid-Base Interaction Enhancing Oxygen Tolerance in Electrocatalytic Carbon Dioxide Reduction. *Angew. Chem. Int. Ed.* 59, 10918–10923. doi:10.1002/anie.202003093

Li, Y., Zhang, K., Yu, Y., Zhan, X., Gui, J., Xue, J., et al. (2022). Pd Homojunctions Enable Remarkable CO_2 Electroreduction. *Chem. Commun.* 58, 387–390. doi:10.1039/d1cc04780a

Li, Z., Yang, Y., Yin, Z., Wei, X., Peng, H., Lyu, K., et al. (2021). Interface-Enhanced Catalytic Selectivity on the C_2 Products of CO_2 Electroreduction. *ACS Catal.* 11, 2473–2482. doi:10.1021/acscatal.0c03846

Lu, X., Jiang, Z., Yuan, X., Wu, Y., Malpass-Evans, R., Zhong, Y., et al. (2019). A Bio-Inspired O_2-Tolerant Catalytic CO_2 Reduction Electrode. *Sci. Bull.* 64, 1890–1895. doi:10.1016/j.scib.2019.04.008

Ma, W., Xie, S., Liu, T., Fan, Q., Ye, J., Sun, F., et al. (2020). Electrocatalytic Reduction of CO_2 to Ethylene and Ethanol through Hydrogen-Assisted C-C Coupling over Fluorine-Modified Copper. *Nat. Catal.* 3, 478–487. doi:10.1038/s41929-020-0450-0

Mistry, H., Varela, A. S., Bonifacio, C. S., Zegkinoglou, I., Sinev, I., Choi, Y.-W., et al. (2016). Highly Selective Plasma-Activated Copper Catalysts for Carbon Dioxide Reduction to Ethylene. *Nat. Commun.* 7, 12123. doi:10.1038/ncomms12123

Suen, N.-T., Kong, Z.-R., Hsu, C.-S., Chen, H.-C., Tung, C.-W., Lu, Y.-R., et al. (2019). Morphology Manipulation of Copper Nanocrystals and Product Selectivity in the Electrocatalytic Reduction of Carbon Dioxide. *ACS Catal.* 9, 5217–5222. doi:10.1021/acscatal.9b00790

Sun, Q., Ren, W., Zhao, Y., and Zhao, C. (2021). Gram-scale Synthesis of Single-Atom Metal-N-CNT Catalysts for Highly Efficient CO_2 Electroreduction. *Chem. Commun.* 57, 1514–1517. doi:10.1039/d0cc07263j

Wang, W., Ning, H., Yang, Z., Feng, Z., Wang, J., Wang, X., et al. (2019). Interface-induced Controllable Synthesis of Cu_2O Nanocubes for Electroreduction CO_2 to C_2H_4. *Electrochimica Acta* 306, 360–365. doi:10.1016/j.electacta.2019.03.146

Wang, Y., Chen, Z., Han, P., Du, Y., Gu, Z., Xu, X., et al. (2018). Single-Atomic Cu with Multiple Oxygen Vacancies on Ceria for Electrocatalytic CO_2 Reduction to CH_4. *ACS Catal.* 8, 7113–7119. doi:10.1021/acscatal.8b01014

Wu, D., Dong, C., Wu, D., Fu, J., Liu, H., Hu, S., et al. (2018). Cuprous Ions Embedded in Ceria Lattice for Selective and Stable Electrochemical Reduction of Carbon Dioxide to Ethylene. *J. Mat. Chem. A* 6, 9373–9377. doi:10.1039/c8ta01677a

Yan, X., Chen, C., Wu, Y., Liu, S., Chen, Y., Feng, R., et al. (2021). Efficient Electroreduction of CO_2 to C_{2+} Products on CeO_2 Modified CuO. *Chem. Sci.* 12, 6638–6645. doi:10.1039/d1sc01117k

Yuan, J., Zhang, J.-J., Yang, M.-P., Meng, W.-J., Wang, H., and Lu, J.-X. (2018). CuO Nanoparticles Supported on TiO_2 with High Efficiency for CO_2 Electrochemical Reduction to Ethanol. *Catalysts* 8, 171. doi:10.3390/catal8040171

Zhang, J., Li, Z., Xia, S., Zhang, T., Wang, Y., Wu, Y., et al. (2021). Reconstructing Two-Dimensional Defects in CuO Nanowires for Efficient CO_2 Electroreduction to Ethylene. *Chem. Commun.* 57, 8276–8279. doi:10.1039/d1cc03171f

Zhao, Z.-H., Zheng, K., Huang, N.-Y., Zhu, H.-L., Huang, J.-R., Liao, P.-Q., et al. (2021). A Cu(111)@metal-Organic Framework as a Tandem Catalyst for Highly Selective CO_2 Electroreduction to C_2H_4. *Chem. Commun.* 57, 12764–12767. doi:10.1039/d1cc05376k

Zhu, C., Wei, X., Li, W., Pu, Y., Sun, J., Tang, K., et al. (2020). Crystal-plane Effects of $CeO_2\{110\}$ and $CeO_2\{100\}$ on Photocatalytic CO_2 Reduction: Synergistic Interactions of Oxygen Defects and Hydroxyl Groups. *ACS Sustain. Chem. Eng.* 8, 14397–14406. doi:10.1021/acssuschemeng.0c04205